The Plasticins: Membrane Adsorption, Lipid Disorders, and Biological Activity[†]

Chahrazade El Amri,*,‡ Claire Lacombe,‡ Karel Zimmerman,§ Ali Ladram,‡ Mohamed Amiche,‡ Pierre Nicolas,‡ and Francine Bruston‡

Peptidome de la peau d'amphibiens, FRE 2852, CNRS, Université Pierre et Marie Curie (Paris-6), Tour 43, 2 Place Jussieu, 75251 Paris Cedex 05, France, and Université Paris 6-Jussieu, INRA, Unité MIG (Mathématique, Informatique and Génome), 78352 Jouy-en-Josas Cedex, France

ABSTRACT: The present study investigates the relationships between structural polymorphism, adsorption onto membrane mimetic support, lipid disturbance, and biological activity of bactericidal 23-residue, glycine-leucine-rich dermaseptin orthologues from the Phyllomedusinae frog skin, the "plasticins". Biological activities were evaluated using the membrane models DMPG (1,2-dimyristoyl-*sn*-glycero-3-phosphatidyl-glycerol) for prokaryotic membranes and DMPC (1,2-dimyristoyl-*sn*-glycero-3-phosphatidylcholine) for eukaryotic membranes. We performed a conformational analysis of plasticins by molecular simulations and spectroscopic methods and analyzed phospholipid perturbations by infrared spectroscopy. Adsorption onto synthetic model membranes was quantified by surface plasmon resonance. Biological assays including antimicrobial and membrane potential-dissipating activities, together with hemolytic tests and imaging analysis of cytotoxicity, were carried out to clarify the peptide−membrane interactions. Two major groups were distinguished: (i) Neutral plasticins revealed the presence of strong β-structures with the zwitterionic or anionic phospholipid vesicles. They were weakly adsorbed in the range of antibacterial activity concentrations (micromolar). Nevertheless, for millimolar concentrations, they caused perturbations at the interface peptide−DMPG vesicles and in the bilayer alkyl chains, suggesting insertion into bacterial membranes. (ii) Cationic plasticins revealed multiple conformational transitions, including destabilized helix states, β-structures, and disordered states. Peptide−lipid complex densities depended on hydrophobic bond strengths. The most soluble cationic plasticins were strongly adsorbed, with stable peptide−lipid interactions inducing noticeable perturbations of bilayer alkyl chains, pointing out possible insertion into bacterial membranes. In contrast, cytotoxic plasticins were less adsorbed, with less stable peptide−lipid interactions causing membrane dehydration, formation of peptide−membrane hydrogen bonds, and little disturbances of lipid alkyl chains. These characteristics could be compatible with their putative action on intracellular targets leading to apoptosis.

The dermaseptins are a superfamily of defense peptides produced by the skins of South American hylid frogs (family Hylidae, subfamily Phyllomedusinae). These peptides form amphipathic α-helices in nonpolar solvents and in SDS micelles or phospholipid liposomes (*1, 2*). The resulting spatial segregation of polar and nonpolar amino acids on opposing surfaces of the helix long axis permits the insertion of a well-defined hydrophobic sector into the membrane lipid bilayer, leading to disruption of the membrane once a critical peptide concentration is reached. Antimicrobial peptides (AMPs)[1] can be classified according to their amino acid composition and 3D structure. There are three main classes: (i) linear peptides forming amphipathic and hydrophobic α-helices, (ii) open-ended cyclic peptides with one or more disulfide bonds, which form β-sheet or α-helix/β-sheet structures, and (iii) peptides with an overabundance of amino acids such as proline and/or glycine. This last class includes glycine-rich peptides. The glycine residues in one of them, clavanin, an antimicrobial peptide isolated from the hemocytes of the tunicate *Styela clava,* are functionally important. At special positions, they act as flexible hinges, so facilitating the insertion of the hydrophobic N-terminal end into the lipid bilayer (*3*). Another glycine-rich antimicrobial peptide, acanthoscurrin, was recently isolated from the hemocytes of the spider *Acanthoscurria gomesiana* (*4*). Glycine-rich peptides also protect plants against fungal pathogens (*5*).

We have studied two natural peptide orthologues from the dermaseptins isolated in our laboratory. One is the cationic peptide PBN2 KF, previously named DRP-PBN2, which has a net charge of +3; it was isolated from *Phyllomedusa bicolor*. Its sequence (GLVTSLIKGAGKLLGGLFGSVTG-NH$_2$) contains two lysines (positions 8 and 12) and one

* Address correspondence to this author. Tel: 33 + 1 44 27 69 52. Fax: 33 + 1 44 27 59 94. E-mail: elamri@ccr.jussieu.fr.
‡ FRE2852, CNRS-UPMC (Paris 6).
§ INRA, Unité MIG.

[1] Abbreviations: AMPs, antimicrobial peptides; ATR-FTIR, attenuated total reflectance FTIR; CD, circular dichroism; CM5, hydrophilic biosensor; diS-C$_3$(5), 3,3′-dipropylthiadicarbocyanine; DMPC, 1,2-dimyristoyl-*sn*-glycero-3-phosphatidylcholine; DMPG, 1,2-dimyristoyl-*sn*-glycero-3-phosphatidylglycerol; FTIR, Fourier transform infrared; GL, glycine−leucine; HPA, hydrophobic biosensor; L1, liposome biosensor; LUVs, large unilamellar vesicles; MIC, minimal inhibitory concentration; PBS, phosphate-buffered saline; PI, propidium iodide; SPR, surface plasmon resonance; TFA, trifluoroacetate; TFE, trifluoroethanol.

Table 1: Primary Structures of Plasticins[a]

PBN2KF	GLVTSLI**K**$_8$GAG**K**$_{12}$LLGGL**F**$_{18}$GSVTG$_a$	⎫
ANCKF	GLVTGLL**K**$_8$TAG**K**$_{12}$LLG**D**L**F**$_{18}$GSLTG$_a$	Cationic plasticins
PD36KF	GVVT**D**LL**K**$_8$TAG**K**$_{12}$LLGN**L**F$_{18}$GSLSG$_a$	
PD36K	GVVT**D**LL**K**$_8$TAG**K**$_{12}$LLGNL**V**$_{18}$GSLSG$_a$	⎭
PD36	GVVT**D**LL**N**$_8$TAG**G**$_{12}$LLGNL**V**$_{18}$GSLSG$_a$	⎫ Neutral plasticins
ANCF	GLVTGLL**N**$_8$TAG**G**$_{12}$LLG**D**L**F**$_{18}$GSLTG$_a$	⎭

[a] All of these peptides were enriched in glycine (21−30%) and leucine (20−30%).

phenylalanine (position 18). The other, PD36, previously named DRP-PD3-6 (6) devoid of positive charges, is neutral (GVVTDLLNTAGGLLGNLVGSLSG-NH$_2$) and was isolated from *Pachymedusa dacnicolor*. We also studied the synthetic peptide ANC F, GLVTGLLNTAGGLLGDLF-GSLSG-NH$_2$, reconstructed from the ancestral proteins, deduced from the sequences of their descendants (7). The PD36 K and PD36 KF analogues of PD36 and the ANC KF analogue of ANC F were synthesized by replacing residues at position 8 with K, at position 12 with K, and at position 18 with F if necessary (Table 1). All of these peptides have very similar sequences, hydrophobicities, and amphipathicities but differ markedly in their spectrum of activity. The peptide structures and interactions with anionic and zwitterionic model membranes were previously investigated by circular dichroism and surface plasmon resonance with DMPC or DMPG vesicles and immobilized bilayers (2). These peptides were shown to adopt an amphipathic α-helical structure in the membrane environment. Positively charged and neutral peptides were hemolytic, whereas only cationic ones had great antimicrobial activity against a broad spectrum of microorganisms. The selection of anionic or zwitterionic membranes appeared to be driven mainly by hydrophobic interactions and short-range electrostatic interactions that prolonged the residence time of the membrane-inserted peptides.

This present study investigates the relationships between structural polymorphism, membrane adsorption, lipid disturbance, and biological activity of these peptides. We first performed a detailed conformational analysis of these peptides by molecular simulations and spectroscopic methods (CD and FTIR). Their adsorption onto both synthetic model membranes (hydrophobic and hydrophilic surfaces) and zwitterionic (DMPC) or anionic (DMPG) mimetic membranes was quantified by SPR. The phospholipid perturbations occurring during the interaction were analyzed by FTIR spectroscopy. Biological assays including antimicrobial and membrane potential-dissipating activities, together with hemolytic tests and imaging analysis of cytotoxicity, were performed in order to obtain further details of the peptide−membrane interactions. The structural polymorphism of these GL-rich dermaseptins (hence the name "plasticins"), investigated on the various surfaces, led to different disturbances of lipid packing affecting either the polar headgroups or the bilayer core. These features were used to interpret their antimicrobial activity and toxicity for prokaryotic and eukaryotic cells.

MATERIALS AND METHODS

Solid-Phase Peptide Synthesis. PBN2 KF, PD36, and ANC F GL-rich peptides and PD36 K, PD36 KF, and ANC KF analogues (Table 1) were synthesized by solid-phase FastMoc chemistry on an Applied Biosystems 433A automated peptide synthesizer (Applera, France) as previously described (2). Fmoc-protected amino acids and resins were from Senn Chemicals (Switzerland) and solvents from sds (France).

Molecular Dynamics Simulation. MD simulations (MDS) were carried out in the canonical ensemble (NVT) using the program Discover 3 (Accelrys, formerly Molecular Simulations, San Diego, CA). Each peptide was initially built in an ideally helical structure. Multiple MD simulations were performed in nonpolar mimetic media using a CVFF force field (8). The nonpolar environment (mimicking to a membrane environment) was imposed by using a value of 5 for the dielectric constant. Once energy had been minimized, molecular simulations were carried out for 1 ns at 300 K in the NVT ensemble. The integration time step in the MD simulations was 2 fs. Snapshots of the trajectories were saved every 10 ps. Trajectories were analyzed using the Analysis module of the Insight II package. Calculations were carried out on a Silicon Graphics O$_2$ R10000 workstation.

Preparation of Phospholipid Vesicles. DMPC (1,2-dimyristoyl-*sn*-glycero-3-phosphatidylcholine) and DMPG (1,2-dimyristoyl-*sn*-glycero-3-phosphatidylglycerol) were purchased from Avanti Polar Lipids. Phospholipid vesicles were prepared by extrusion as indicated in ref 2.

CD Spectral Analysis. As the components of plasticin CD spectra could not be estimated with any of the available commercial or academic software, we developed a spectral decomposition method with the construction of standard spectra (see Supporting Information). Briefly, 126 spectra (NPEP = 126) were measured at 1 nm intervals over the range 190−250 nm (61 values per peptide) in PBS, DMPC, and DMPG media (2). Moreover, PD36 dissolution was realized in water in order to allow comparison with IR data. The component spectra were deduced by the least-squares fit method. A minimizer (eq 1) was written in Scilab using the Newton method with the Marquardt algorithm and parabolic line search (http://www.scilab.org). Data overfitting was avoided (9) using a truncated harmonic series (eq 2).

$$\min \sum_{npep=1}^{NPEP} \sum_{\lambda=190}^{250} \left[\epsilon_{npep}(\lambda) - \sum_{M=1}^{NCOMP} c_{npep,M} \epsilon_M(\lambda) \right]^2 \quad (1)$$

$$\epsilon_M(\lambda) = \sum_{n=0}^{NHARMON} \left\{ w_{M,n}^{(s)} \sin\left[\frac{2\pi n}{250-190} (\lambda - 190) \right] + w_{M,n}^{(c)} \cos\left[\frac{2\pi n}{250-190} (\lambda - 190) \right] \right\} \quad (2)$$

Four components were constructed, and only three were attributed; one was assigned to α-helix, one to random coil, and one to β-related structures (E1, E2, and E3).

FTIR Measurements. The trifluoroacetate (CF$_3$COO$^-$) counterions that strongly associated to the peptides were exchanged for chloride ions by lyophilizing them in 80 mM HCl. This eliminated the strong C=O stretching band of the CF$_3$COO$^-$ anions centered at 1673 cm^{-1} from the peptide amide I absorption range (10).

The amide NH/ND-exchange experiments were performed on a Bruker Equinox 95 IR 850 spectrometer equipped with a crystal support and a MCT detector. Each spectrum included 100 coadded scans at a resolution of 4 cm^{-1} with one level of zero filling and a boxcar apodization. A lyophilized grain of each peptide was hydrated with D$_2$O for 5 min; spectra were recorded and analyzed.

Transmission experiments were carried out on lyophilized GL-rich plasticins (2 mM) dissolved first in D$_2$O and then in deuterated phosphate buffer (50 mM Na$_2$DPO$_4$) adjusted to pD 7 with DCl or in 20 mM DMPC or DMPG solution extruded in the same buffer. Spectra were recorded on a Perkin-Elmer Model 1720 Fourier transform spectrometer at room temperature in dried air with a resolution of 4 cm^{-1}. Transmission spectra were obtained using an IR cell with CaF$_2$ windows and a 50 μm spacer. The HOD contribution was minimized by subtracting a reference HOD spectrum. The effects of plasticins on lipids in the 2800−3000 cm^{-1} domain and lipids on peptides in the 1500−1800 cm^{-1} domain were established by stepwise spectral subtractions.

Determination of Secondary Structure. The spectra of the amide I′ band have been correlated with the secondary structures in numerous studies (*10−13*). Second derivative analyses revealed that this 1580−1720 cm^{-1} region involved five overlapping component bands (1624, 1637, 1650, 1665, and 1685 cm^{-1}) representing different states of hydration and specific peptide secondary structures. The amide I′ spectral region 1620−1635 cm^{-1} was attributed to H-bonded β-sheeted structures, while the 1635−1660 cm^{-1} domain was attributed to random coil structures involving peptide carbonyls directly solvated by water and α-helix structure (*14, 15*). The 1660−1690 cm^{-1} region was related to weakly solvated or unsolvated peptide carbonyls.

The lipid CO ester in the spectral decomposition of the 1680−1780 cm^{-1} domain gave maximum components at 1727 and 1742 cm^{-1} for DMPC and 1726 and 1743 cm^{-1} for DMPG, close to published data (*16−18*). These two main bands are attributed in the literature to hydrogen-bonded (hydrated) carbonyl groups and free (anhydrous), respectively (*19*).

The lipid (CH) stretching contribution in the 2800−3000 cm^{-1} spectral region was characterized by four bands, two strong bands (2850 and 2920 cm^{-1}) assigned to the symmetric and antisymmetric methylene stretching modes and weaker bands (2872 and 2956 cm^{-1}) assigned to the symmetric and antisymmetric methyl stretching modes (*17*).

The spectral ranges of conformational interest, the amide I′ band, the lipid CO ester, and the lipid (CH) stretching bands, were analyzed using the ASREL program to optimize the amplitudes, band positions, half-width, and composition of the individual bands of a sum of Gaussian/Lorentzian profiles for the amide I′ band and Lorentzian profiles for the lipid (CH) stretching mode. Curves were fitted using the PAMIR program to calculate the relative abundance of structural contributions for both peptide and lipid in the various set of experiments (transmission and ATR).

Surface Plasmon Resonance. Peptides were adsorbed onto a hydrophobic surface (HPA) or to a hydrophilic surface (CM5), and interactions were monitored with a BIAcore 2000 (BIAcore, Uppsala, Sweden). The HPA biosensor was composed of octadecanethiol covalently grafted to the gold surface to give a hydrophobic monolayer (*20*). The CM5 biosensor was a carboxymethylated dextran matrix which produced a hydrophilic, negatively charged surface (COO$^-$ groups). The binding of the peptides to the bilayer membrane with DMPC or DMPG on sensor chip L1 was also measured. The L1 sensor chip was composed of a carboxymethylated dextran matrix which yielded a hydrophilic negatively charged surface (COO$^-$ groups) modified with lipophilic compounds. All experiments were performed at 25 °C in running phosphate-buffered saline (50 mM, NaH$_2$PO$_4$/Na$_2$-HPO$_4$, pH 7, 150 mM NaCl) that had been degassed and passed through a 0.22 μm filter. Peptides were diluted from 0.5 to 30 μM. Layouts were obtained at a flow rate of 20 μL·min^{-1} to avoid limitation by mass transport (*21*). The L1 and HPA biosensors were regenerated by repeated injections of the nonionic detergent (40 mM *n*-octyl D-gluco-pyranoside, 100 μL) at a flow rate of 10 μL·min^{-1} until the initial baseline was reached. The CM5 surface was regenerated by injecting 10 mM NaOH (50 μL, 100 μL·min^{-1}).

Adsorption onto Membrane Bilayers. Supported DMPC or DMPG bilayers were formed on the surface of an L1 chip (*22*) by injecting LUVs (60 μL, 0.5 mM) in PBS (50 mM, 150 mM NaCl, pH 7, 25 °C) at a low flow rate (2 μL·min^{-1}). This produced a signal of ∼4400 resonance units (RU) for the two lipids after the non-phospholipid-coated chip was removed by a pulse (12 s) of 100 mM NaOH. Each peptide was diluted (1−30 μM), and 60 μL was immediately injected at a flow rate of 20 μL·min^{-1}. Only the layouts obtained after the formation of a bilayer membrane corresponding to approximately 4400 ± 300 RU were retained. Kinetics were measured with a 3 min adsorption step followed by 3 or 10 min desorption steps.

Antimicrobial Assays. Gram-positive eubacteria and Gram-negative eubacteria were cultured as described previously (*2*) using HEPES buffer (5 mM HEPES, 5 mM glucose, pH 7.2) instead PBS. The antimicrobial activity was monitored by incubating 10 μL of each peptide (0.2−100 μM) with an inoculation (100 μL/well, OD 0.05) from an overnight culture of two Gram-positive (*Staphylococcus aureus* ATCC 25923, *Bacillus megaterium* ATCC 9885) or three Gram-negative (*Escherichia coli* 363 ATCC 11775, *Salmonella typhimurium* CIP 6062, *Enterobacter cloacae* ATCC 13047) bacteria. The 96-well untreated microtitration plates (Nunc F96) were incubated at 37 °C overnight, and the absorbance at 630 nm was measured by an ELISA reader (*23*). Minimal inhibitory concentrations (MICs) were determined; MIC was defined as the dose producing 100% inhibition of growth. Control incubations with 10 μL formaldehyde were used to monitor the validity of the assays.

Hemolysis of Rat Red Blood Cells. The hemolytic activity of the peptides was determined using fresh rat erythrocytes. The blood was centrifuged, and the erythrocytes were rinsed three times with PBS (50 mM phosphate buffer and 0.15 M NaCl at pH 7.4). Peptides were incubated with suspended erythrocytes (4% v/v in PBS) at 37 °C for 60 min, and the cells were then removed by centrifugation at 1500*g* for 5 min at 4 °C. Hemolysis was assessed by measuring the optical density at 540 nm of the supernatant. Erythrocytes lysed with 1% Triton X-100 were used to produce 100% hemolysis.

Membrane Activity Assay. The effect of the peptides on the membrane integrity was tested using the fluorescent membrane potential-sensitive probe 3,3′-dipropylthiadicar-

bocyanine iodide [diS-C$_3$(5)] (Molecular Probes-Invitrogen) (*24*, *25*). *E. coli* 363 ATCC 11775 was grown at 37 °C to mid-logarithmic phase, washed two times with HEPES buffer (see above) at 4 °C, and suspended in the same buffer containing 1 μM diS-C$_3$(5) at an OD$_{600}$ of 0.05. This probe concentration was not toxic for the strain. The fluorescence emission was monitored at 37 °C using a Perkin-Elmer LS 50B spectrofluorometer with Spectro Winlab software at 670 nm (excitation at 620 nm). The desired concentration (5−75 μM) of test peptide was added once the dye uptake was maximal, as indicated by a stable reduction in fluorescence due to quenching of the accumulated dye in the membrane interior. The membrane potential was fully dissipated with Triton X-100 (0.05% final concentration). The membrane potential-dissipating activity of the peptides is expressed as the percent inhibition: in HEPES−glucose, F_0 is the stable fluorescence after adding the diS-C$_3$(5) probe, F_P is the fluorescence 10 min after adding the peptide, and F_T is the fluorescence after adding Triton.

Hela Cell Culture and Videomicroscopy. Hela cells were cultivated in 12-well plates (350000 cells per well) in RPMI 1640 medium (Invitrogen) without phenol, supplemented with 5% fetal calf serum (FCS) in a 5% CO$_2$ atmosphere for 24 h. Cells were grown in serum-free RPMI medium for live cell imaging. The cells were imaged by phase contrast using a DM IRBE microscope (Leica) with 63× objective (NA = 0.7), a condenser (working distances: 23 mm, NA 0.53), and a coolsnap-cooled CCD camera (Ropper Scientific). Metamorph 4.7 was used for computer-based image acquisition. The images obtained at 0 and 24 h for control cells and samples with 10 μM peptides PBN2 KF or ANC KF were spiced with Image J (http://rsb.info.nih.gov/ij/download.html). Apoptotic bodies were discriminated from normal cells by the Hoechst/propidium iodide (PI) technique. Cells were incubated with Hoechst 33342 (12.5 μg·mL^{-1}) and PI (5 μg·mL^{-1}) for 5 min and then examined under an inverted fluorescence microscope.

RESULTS

Conformational Plasticity As Indicated by Molecular Dynamics Simulation. Several molecular dynamic simulations (MDS) were performed on the six GL-rich plasticins through 1 ns, starting from an ideal α-helix in a nonpolar mimetic ($\epsilon = 5$) medium as preliminary conformational analysis, to assess the variability in the structural transitions. The Cα−Cα distance between N- and C-terminal residues was used to identify folded structures (Figure 1). Two behaviors were observed: neutral peptides underwent transitions between three conformations (helix/coil/β-structure), while cationic peptides underwent various transitions between two states. PBN2 KF oscillated between helix and disturbed helix, while PD36 K and ANC KF underwent classical helix−coil transition, and PD36 KF was found to be the most foldable within β-hairpin-related structures. This is the first indication of differences in the structural plasticity between these peptides.

Aggregation and Conformation of the Plasticins in Aqueous Environment. The NH/ND-exchange kinetics obtained by ATR-FTIR was used to assess peptide structural transitions and self-association. Solid state was taken as 100% NH content for the NH/ND-exchange analysis. Figure 2

showed that cationic plasticins (PBN2 KF, ANC KF, PD36 K, and PD36 KF) rapidly exchanged 85% of their NH content with ND after incubation in D$_2$O for 10 min. The NHs of neutral plasticins (PD36 and ANC F) and cationic peptide ANC KFbis were exchanged slowly. Ten minutes after removal of the D$_2$O, about 20% of ANC KF hydrogens were exchanged to deuterium, when the peptide was newly resuspended in D$_2$O (ANC KFbis). Its apparent NH content over 100% could be linked to differences in the molar extinction coefficient of β-sheeted structures or peptides in a nonpolar environment (*26*, *27*). Furthermore, a previous CD experiment pointed out a β-structure profile in PBS for ANC KF (*2*).

Analysis of Plasticin Conformation in DMPC or DMPG Vesicles. All FTIR spectra were recorded in deuterated phosphate-buffered saline, pH 7, using 20 mM lipids and 2 mM peptides (molar ratio $R_{P/L} = 1/10$); CD spectra were obtained with concentrations of 300 μM lipids and 30 μM peptides in phosphate buffer, pH 7 (molar ratio $R_{P/L} = 1/10$) (*2*). The amide I′ spectra in the domain 1500−1800 cm^{-1} of the plasticins in DMPC and DMPG are shown in Figure 3. The maximum absorbances of the amide I′ bands were observed at 1645 ± 1 cm^{-1}. Analysis of the amide I′ bands for all plasticins was performed with a unique decomposition "procedure" allowing pragmatic band-to-band and peptide to peptide comparisons and was consistent with a mixture of random, α-helix, and β-related structures. Moreover, FTIR analysis allowed the peptide carbonyl assignments (hydrated, H-bonded, and unsolvated).

Previous CD spectra showed that all cationic peptides, except PD36 KF, had very little ordered structure in buffered solution, while neutral peptides displayed β-structures (*2*). The conformational analyses and component band distributions were reconsidered and attributed. Two main groups were considered: α-helical with disordered structures and β-related structures (β-sheet, bent, or turn). The unsolvated peptide carbonyls (1665−1685 cm^{-1}) were gathered with H-bonded peptide carbonyls according to refs *11* and *15*.

Table 2 shows a good correlation between the β-structure contents of plasticins on the two mimetic membrane surfaces by both techniques, when α-helix + coil contents deduced from the CD data and α-helix + hydrated peptide carbonyls derived from IR data were gathered. In contact with DMPC or DMPG vesicles, cationic plasticins exhibited about 25% β-structure contents except PD36 KF that presented 40% β-structure contents in DMPG; estimated α-helix contents obtained from CD data varied from 28% to 52%. Neutral plasticins presented greater β-related structure contents: 45% for ANC F and 57% for PD36 suspended directly in buffer. The mismatch observed for PD36 was attributed to differences in solubilization procedures used for CD and IR. PD36 dissolved directly in water presented a random coil profile, whereas it adopted β-sheeted structures after 3 days in an unstirred quartz cuvette (results not shown).

Adsorption onto Synthetic Surfaces in Flow Experiments by SPR. Surface plasmon resonance (SPR) provides information on kinetics of the interactions between a peptide and the adsorbing surface in real time (*21*). SPR response (a change in resonance signal), expressed as response units (RU), depends on the density of the peptide adsorbed onto the surface. Correlation between RU and adsorbed mass is about 1000 RU for 1 ng of biomolecules.mm^{-2}. The density
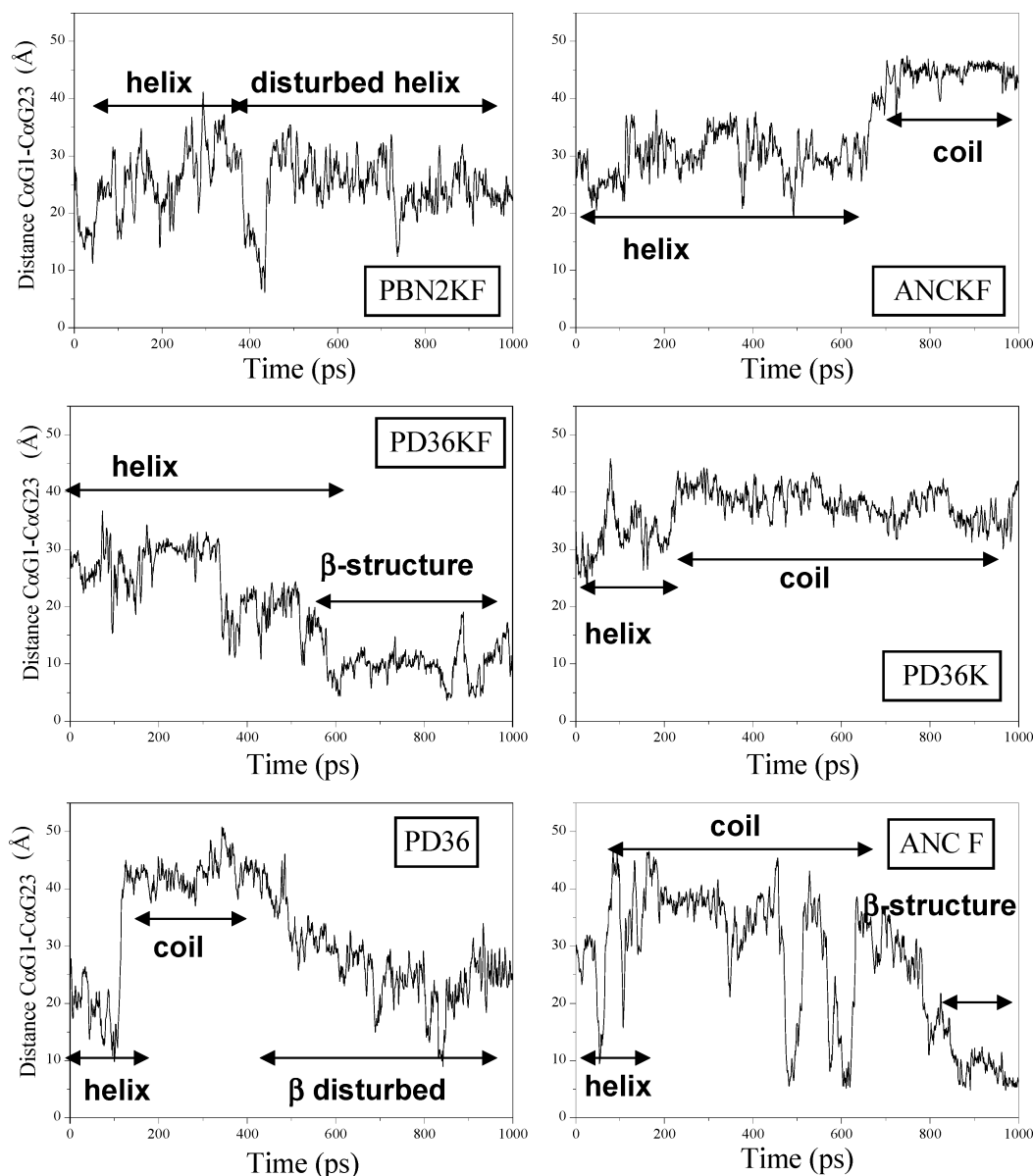
FIGURE 1: 1 ns molecular dynamics trajectories of the Cα–Cα distances between N- and C-terminal residues for Gly-Leu-rich peptides in nonpolar mimetic medium ($\epsilon = 5$). β-Structures were characterized by 6–10 Å distances, helices by 25–35 Å, and random coils by 40–50 Å.

of each peptide adsorbed onto synthetic surfaces was quantified in continuous flow assuming the manufacturer characteristics for the detection surface (1.2 mm^2).

SPR signals (RU) for peptide PBN2 KF adsorbed on the plane and rigid hydrophobic surface (HPA) were plotted against time (Figure 3A) or expressed as adsorption density (ng·mm^{-2}) at 180 s as a function of peptide concentration (Figure 3B). For all plasticins, concentrations below 5 μM failed to produce complete irreversible coverage of the hydrophobic HPA sensor chip in 180 s. Relative responses at the adsorption plateau varied from 580 to 800 RU at a peptide concentration of 30 μM (Table 3). For a peptide molecule considered as a perfect 23-residue α-helix, its contact surface should be regarded as a rectangle measuring 3.3 nm long by 1.5 nm wide, giving a surface area of ~5 nm^2. A peptide that is entirely in an extended or β-hairpin structure would have a contact surface area of 10–12 nm^2. Consequently, the hydrophobic surface could receive 0.9 ng of helical peptide but only 0.4 ng of a peptide presenting

alternative conformation. Experimental adsorption densities for the peptides devoid of K (~0.5 ng·mm^{-2}) were close to the calculated values for extended or β-structures (Table 3). The average maximal adsorption densities for cationic KF peptides (PBN2 KF, ANC KF, and PD36 KF) were 0.7 ng·mm^{-2}, raising from mixed α-helix and β-like structure with a predominance of the helix; values of PD36 K devoid of F were nearer those of neutral peptides, suggesting a larger content of β-like structures.

Maximum SPR response for hydrophilic surfaces (CM5 biosensor) was obtained at 30 μM and depended on the presence of K and F residues (Table 3). The scale of adsorption densities was ANC KF > PBN2 KF > PD36 KF > PD36 K $\gg$ neutral peptides. The intense adsorption density of cationic peptides (1.2–4.1 ng·mm^{-2}) included multiple layers that were easily desorbed by buffer (data not shown). The two neutral plasticins, in contrast, were weakly adsorbed (~0.15 ng·mm^{-2}), ANC F reversibly and PD36 irreversibly.
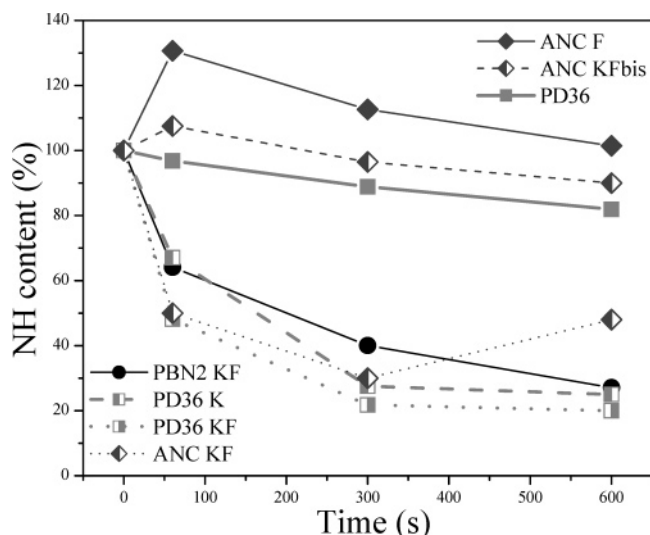
FIGURE 2: NH content (in percent) of the plasticins measured by ATR-FTIR on a crystal surface. The reference 100% was the NH band area of the peptide solid state. The ANC KFbis was obtained by a new hydration after primary D_2O evaporation. The standard error was 1%.

Table 2: Distributions of Component Bands between CD Data and FTIR Data in Two Lipid Environments[a]

	CD			CO amide I′ (FTIR)	
	α-helix + coil	hydrated	β-sheet + β-turn	hydrated	H-bonded + unsolvated
DMPC					
PBN2 KF	31 + 45	76	24	69	31
ANC KF	28 + 46	74	26	74	26
PD36 KF	42 + 37	79	21	79	21
PD36 K	38 + 36	74	26	73	27
PD36	14 + 29[b]	43[b]	57[b]	nd	nd
	45 + 30[c]	75[c]	25[c]	78	22
ANC F	23 + 33	56	44	55	45
DMPG					
PBN2 KF	40 + 33	73	27	76	24
ANC KF	35 + 36	71	29	70	30
PD36 KF	47 + 07	54	46	61	39
PD36 K	52 + 34	76	24	78	21
PD36	48 + 14	62	38	62	38
ANC F	28 + 29	57	43	55	45

[a] α-Helix and random coil contributions obtained by CD were compared to hydrated peptide carbonyl contents by FTIR. β-Structure contents (sheet, bent, or turn) measured by CD were grouped together and compared to percentages of H-bonded and unsolvated peptide carbonyl obtained by FTIR. The peptide/lipid molar ratio in both experiments was 1/10. Peptide concentrations were 30 μM for CD and 2 mM for FTIR. The standard error was 1%. The column hydrated corresponds to the sum (α-helix + coil). [b] CD experiments were realized for PD36 in buffer. [c] CD experiments were realized for PD36 in water.

Adsorption of Plasticins onto a Lipid Bilayer As Determined by SPR. The rates at which each peptide was adsorbed onto DMPC or DMPG bilayers were measured in real time and analyzed by BIAevaluation (*2*). Previous SPR results were reevaluated using mainly molecular adsorption densities instead of kinetic constants (Table 4).

Cationic plasticins were readily adsorbed onto DMPC and DMPG bilayers, giving very high adsorption densities. These densities were greater than those observed on the hydrophobic surface and similar to those obtained on the negative surface (CM5 biosensor). The densities of cationic peptide molecules stacked on the DMPG bilayer were close, about 3.0 ± 0.5 ng·mm^{-2} at bulk peptide concentrations greater

than 5 μM. However, they markedly differed in their binding to the DMPC bilayer, varying from 1 to 4.0 ± 0.5 ng·mm^{-2}, underlying the formation of multiple layers (Table 4). Binding to DMPC always appeared to be weaker but was nevertheless present. Adsorption densities at the end of desorption phase (180 s) varied with the peptide concentration, sequence, and phospholipid specificity (*2*). However, the peptide density immobilized on the phospholipids after 10 min of desorption, named PL* complex, showed that the DMPC headgroups partially prevented the anchorage of cationic plasticins, except for ANC KF.

The lipid/peptide molecular ratios for cationic plasticins varied greatly between the two membrane models (Table 4, data in parentheses). The molecular ratios on the DMPG bilayer were found identical for all cationic peptides (*2*), whereas on the DMPC bilayer, PBN2 KF revealed a greater ratio (*5*) than ANC KF (*3*); the smaller ratios were obtained for the PD36s (*1*).

The adsorption densities for neutral PD36 and ANC F on both the DMPC and DMPG bilayers were about ten times lower than those for the cationic peptides (Table 4). The L/P molecular ratio was 20 for ANC F on both surfaces, while it differed for PD36 on the zwitterionic bilayer (30) and on the anionic bilayer (60).

Effects of Plasticins on the Lipid–Solvent Interface As Examined by FTIR. The stretching vibration mode of the lipid carbonyl groups [ν(CO)] provided details on the hydration, environment, and conformation of the membrane interface region. The modulation of CO vibration by the various peptides provided information on the hydration of the polar–nonpolar interface of the lipid bilayer and on the hydrogen bonding of the lipid with the peptide. The two peptides PBN2 KF and ANC KF (and to a lesser extent PD36 KF) caused redistribution of the components in DMPC vesicles, with higher 1727/1742 ratios compared to pure DMPC (Table 5). Binding of all the plasticins decreased the 1726/1743 ratio of DMPG vesicles to below that of pure DMPG, in contrast to their effects on the zwitterionic membrane (Table 5). All of the difference spectra for DMPG vesicles shown in Figure 2 had a hump centered at 1750 cm^{-1}. This could indicate lipid CO trapping within peptide hydrophobic domains and be correlated with the stability of the PL* complex (Table 4).

Effects of Plasticins on the Alkyl Chain Region As Indicated by FTIR. Spectra in the 2800–3000 cm^{-1} region were used to deduce the perturbations of the lipid hydrocarbon chain caused by the peptides. Our spectral decomposition gave maxima at 2852, 2875 cm^{-1} and 2923, 2956 cm^{-1} for the symmetric and antisymmetric alkyl stretching modes for both phospholipids (Table 6). All of the plasticins caused no variations in the distribution of the component bands of DMPC ν_S(CH$_2$–CH$_3$) stretching vibration modes, whereas cationic ones and especially PBN2 KF altered the ν_{AS}(CH$_2$–CH$_3$) modes, indicating that these peptides interacted with the bilayer core.

In contrast, strong perturbations were observed with DMPG (Table 6). The symmetrical stretching band was shifted from 2852 cm^{-1} in pure DMPG to just 2853 cm^{-1} for peptides PBN2 KF and ANC KF, whereas these same peptides slightly displaced the antisymmetric stretching band from 2922 to 2924 cm^{-1} (Figure 5). All peptides affected the antisymmetric ν_{AS}(CH) stretching modes differently and
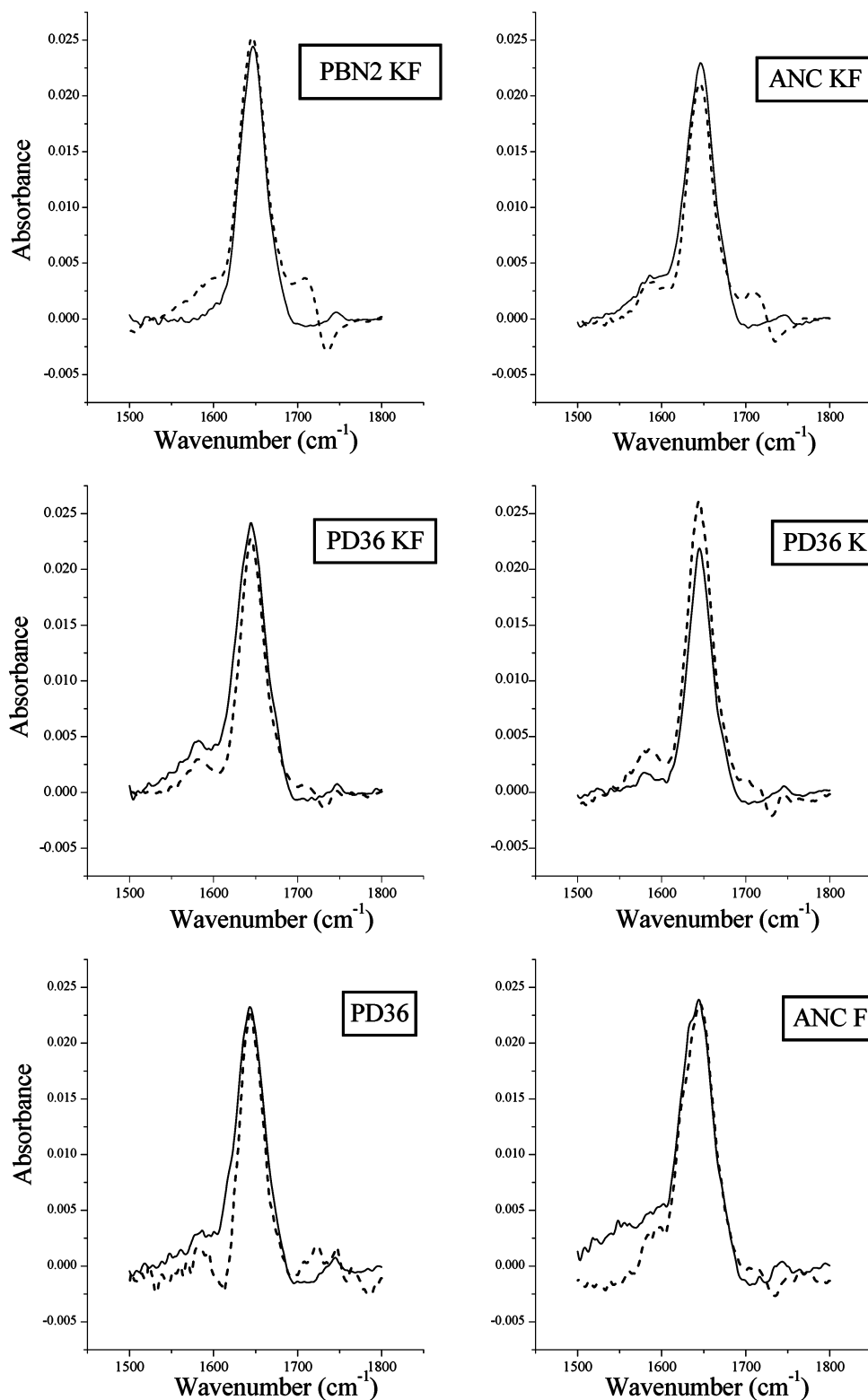
FIGURE 3: Normalized FTIR spectra in the $1500-1800$ cm^{-1} region of plasticins in zwitterionic DMPC vesicles (broken line) and in anionic DMPG vesicles (solid line) at 20 mM lipid and 2 mM peptide. It shows structural changes in the $1680-1780$ cm^{-1} region [ν(CO) of lipids] for PBN2 KF, ANC KF, and PD36 KF due to peptide–DMPC interactions. All of the peptides tested gave rise to peptide–DMPG interactions that disturbed this region of the spectrum.

indicated enhancement of acyl chain flexibility. Distributions of the ν_S(CH) stretching vibration component band, expressed as a percentage, decreased for the three peptides containing two K and one F and increased for the ν_{AS}(CH) component band (Table 6). The ν_S(CH$_2$) also became broader (Figure 5), suggesting greater rotational mobility of the acyl chain.

The distributions of the ν(CH$_3$) vibrations were more dispersed than those of the ν(CH$_2$) vibrations (Table 6). These displacements and redistributions were due to the gel to liquid-crystalline phase transition.

Antimicrobial and Hemolytic Activities. Table 7 presents the relative antimicrobial activities of the plasticins studied

Table 3: Continuous Flow SPR Data Showing the Relationship between Maximum SPR Response at 30 μM and Adsorption Density for Both Synthetic Biosensors (Hydrophobic HPA or Hydrophilic CM5)

peptide (mol wt)	SPR response at 30 μM (RU)		adsorption density (ng·mm^{-2})		adsorbed molecule number·nm^{-2}		immobilized molecule number·nm$^{-2 a}$	
	HPA	CM5	HPA	CM5	HPA	CM5	HPA	CM5
PBN2 KF (2144)	800	3250	0.7	2.7	0.19	0.761	0.19	0.054
ANC KF (2231)	780	4950	0.7	4.1	0.18	1.111	0.18	0.054
PD36 KF (2260)	780	2500	0.7	2.1	0.18	0.551	0.18	0.054
PD36 K (2213)	600	1400	0.5	1.2	0.14	0.331	0.14	0.054
PD36 (2127)	615	225	0.5	0.19	0.15	0.054	0.15	0.054
ANC F (2131)	580	150	0.5	0.12	0.14	0.034	0.14	0.054

^{a} The number of immobilized molecules per nm^2 was evaluated from the SPR response at 180 s in the desorption step.

Table 4: SPR Recapitulative Data Showing Adsorption Densities of Plasticins (30 μM) on Zwitterionic (DMPC) and Anionic (DMPG) Membranes^a

peptide (mol wt)	adsorption density at 30 μM (RU)		adsorbed molecule number·nm^{-2} ($R_{L/P}$)^b		PL* complex density (ng·mm^{-2})^c	
	DMPC	DMPG	DMPC	DMPG	DMPC	DMPG
PBN2 KF (2144)	1400	3400	0.33 (5)	0.79 (2)	0.3	1.2
ANC KF (2231)	2000	4000	0.45 (3)	0.89 (2)	0.5	1.2
PD36 KF (2260)	4400	4200	1.00 (1)	0.90 (2)	0.3	1.2
PD36 K (2213)	5000	3600	1.10 (1)	0.80 (2)	0.2	1.0
PD36 (2127)	200	100	0.05 (30)	0.02 (60)	0.1	nd
ANC F (2131)	300	300	0.07 (20)	0.07 (20)	nd	nd

^{a} The peptide−lipid complex densities (ng·mm^{-2}) were evaluated from the SPR responses 10 min after the start of desorption (nd = not determined). $R_{L/P}$ molecular ratios are in parentheses. ^{b} A lipid bilayer was formed by roughly 3 molecules of phospholipids·nm^{-2}, but only half was a potential adsorption surface for the peptides, i.e., 1.5 molecules.nm^{-2}. ^{c} The PL* complex density (ng·mm^{-2}) was evaluated from the SPR response after 10 min of desorption.

Table 5: Assignment and Distribution of Component Bands (%) for Lipid ν(CO) Stretching Vibrations Resolved in FTIR Spectra Obtained at 2 mM Concentrations of All Plasticins with 20 mM DMPC or DMPG in PBS ($R_{L/P} = 10$)^a

	DMPC (%)			DMPG (%)		
	1727 cm^{-1} hydrogen bond	1742 cm^{-1} dehydrated	1727/1742 ratio	1726 cm^{-1} hydrogen bond	1743 cm^{-1} dehydrated	1726/1743 ratio
without peptide	60.5	39.5	1.5	64.0	36.0	1.8
PBN2 KF (2144)	63.0	37.0	1.7	58.0	42.0	1.4
ANC KF (2231)	62.0	38.0	1.6	60.0	40.0	1.5
PD36 KF (2260)	61.0	39.0	1.6	58.0	42.0	1.4
PD36 K (2213)	60.0	40.0	1.5	59.5	40.5	1.5
PD36 (2127)	60.5	39.5	1.5	59.0	41.0	1.4
ANC F (2131)	60.0	40.0	1.5	60.0	40.0	1.5

^{a} The standard error was 1%. Peptide molecular weights are indicated in parentheses.

Table 6: Assignment and Distribution of Component Bands (%) in CH Stretching Vibration Modes Resolved in FTIR Spectra Obtained for 2 mM Concentrations of All Peptides with 20 mM DMPC or DMPG in PBS ($R_{L/P} = 10$)^a

	cm^{-1}	DMPC	PBN2 KF	ANC KF	PD36 KF	PD36 K	PD36	ANC F
ν_S(CH$_2$)	2852	22.3	22.8	22.1	22.8	22.7	22.5	22.4
ν_S(CH$_3$)	2875	2.0	2.1	2.3	2.1	2.0	2.0	2.1
ν_{AS}(CH$_2$)	2923	66.2	63.8	66.4	65.8	66.9	65.9	66.2
ν_{AS}(CH$_3$)	2956	7.5	7.0	5.5	6.3	5.4	7.5	7.4
	cm^{-1}	DMPG	PBN2 KF	ANC KF	PD36 KF	PD36 K	PD36	ANC F
ν_S(CH$_2$)	2852	21.3	18.4	19.4	20.2	20.6	20.71	22.3
ν_S(CH$_3$)	2875	2.8	4.4	3.6	2.6	3.1	2.61	2.0
ν_{AS}(CH$_2$)	2923	68.2	65.0	64.2	66.3	65.3	64.71	64.5
ν_{AS}(CH$_3$)	2956	4.3	9.1	7.6	5.6	6.0	8.61	6.7

^{a} The standard error is 1%.

on bacteria strains. The four cationic peptides exhibited strong antimicrobial activities in contrast to the two neutral peptides that were found to be inactive against either Gram-negative or Gram-positive strains at concentrations of up to 100 μM. Some Gram-negative strains were resistant to the two cationic PD36s, whereas ANC KF was more potent than PD36 KF against Gram-positive strains, suggesting that the lipopolysaccharide (LPS) environment is implicated. Moreover, all plasticins induced erythrocyte hemolysis (Table 7).

Effect on Membrane Potential Gradient. Transmembrane potential depolarizing experiments were performed to probe the implication of additional factors that may modulate the
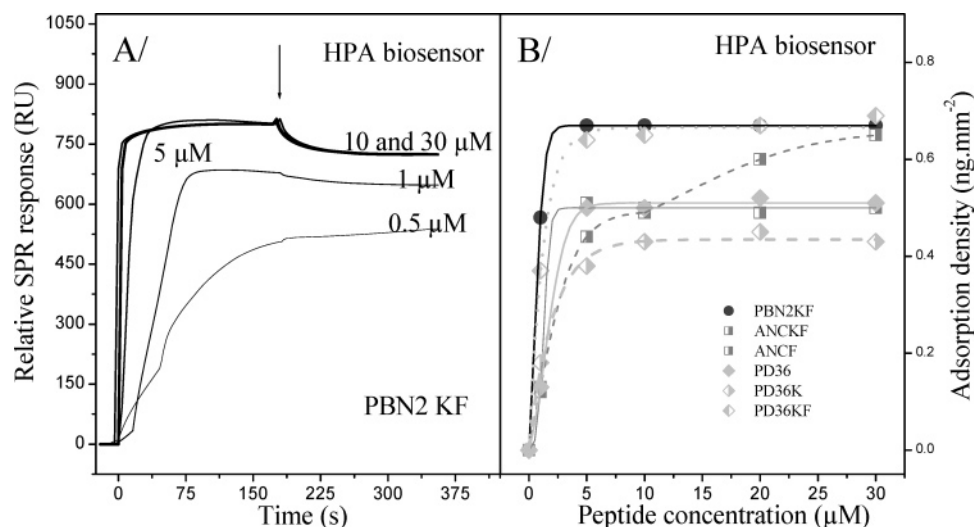
FIGURE 4: Adsorption of plasticins onto synthetic membranes in continuous flow SPR. (A) SPR sensorgrams of peptide PBN2 KF (0.5−30 μM) adsorbed onto a hydrophobic surface (HPA). (B) Adsorption density (ng·mm^{-2}) of all peptides at 180 s versus peptide concentrations on the HPA biosensor. The arrow indicates the start of desorption.
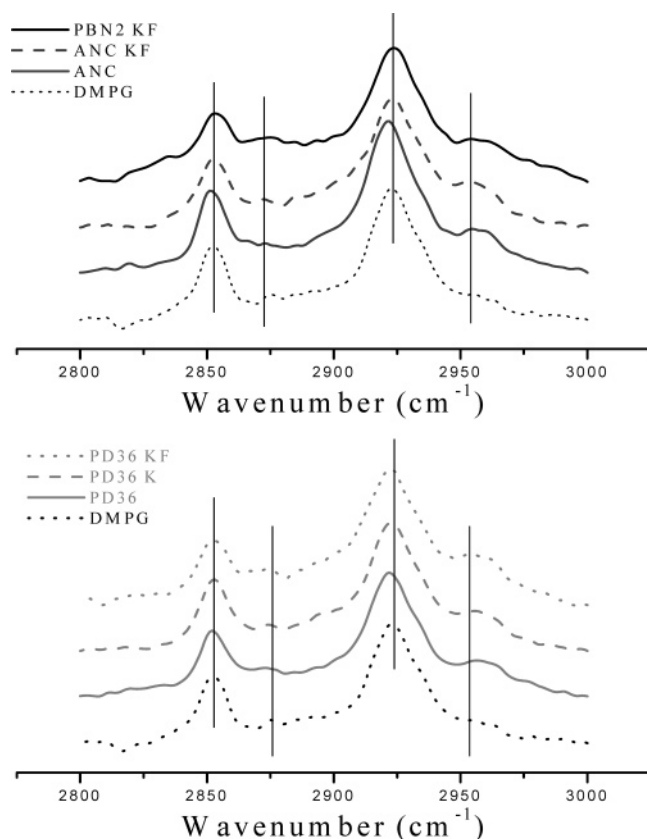

FIGURE 5: Normalized FTIR spectra (2800−3000 cm^{-1}) of plasticins in anionic DMPG vesicles at a lipid/peptide (L/P) molar ratio of 10 (20 mM lipid and 2 mM peptide).

interaction ability with the bacterial plasma membrane as required for antibacterial activity. The fluorescence intensity of diS-C$_3$(5) decreased gradually when it was added to mid-log phase *E. coli* 363 cells at 37 °C until it stabilized at about 10% of its original value after 20 min. Only *E. coli* cells with an intact membrane potential gradient quenched the fluorescence (*28*). Table 8 shows that ANC KF and PD36 plasticins were unable to dissipate the membrane potential at tested concentrations. PD36 KF presented the same dissipation efficiency (100%) as Triton X-100, whereas PBN2 KF, characterized by similar MIC (6.25 μM), dis-

sipated only 50% of the membrane potential. Multiple colonies were counted when 100 μL of the peptide/bacterium mixture was incubated on an LB agar plate overnight, indicating a bacteriostatic effect for ANC KF and PD36 KF. In contrast, PBN2 KF was found to be bactericidal.

Cytotoxicity Studies by Imaging Analysis. The action of the peptides PBN2 KF and ANC KF on Hela cells was used to test our hypothesis that the formation of peptide−membrane complexes could be responsible for the cytotoxicity toward differentiated eukaryotic cells (Figure 6). Incubation of cells with 10 μM peptide for 24 h damaged the plasma membrane and changed the cell morphology; ANC KF caused greater changes than PBN2 KF. Both caused local membrane fusion, the formation of large polynucleated cells, and also altered the nuclei, causing condensation and fragmentation (Figure 6B,C). Apoptotic bodies were observed after 24 h, as revealed with Hoechst/PI staining (Figure 6D). Incubation of cells for a few hours with 100 μM peptide or for 48 h with 10 μM peptide led to necrosis and cell death (result not shown).

DISCUSSION

Plasticins belong to a group of dermaseptin-related peptides characterized by close GL-rich sequences and hydrophobicities (*2*). The present work shows that, in contrast to classical amphipathic cationic AMPs, the plasticins displayed structural polymorphism (Figure 1) leading to discrepancies in biological activities. The net charge of biomembranes is mainly due to their phospholipid stoichiometry and structure. Cell membranes composed predominantly of phosphatidylglycerol (PG), cardiolipid (CL), or phosphatidylserine (PS) tend to be highly electronegative; such compositions are found in many bacterial pathogens (*29*). On the contrary, a bilayer rich in the zwitterionic phospholipids, phosphatidylethanolamine (PE) and phosphatidylcholine (PC), commonly found in mammalian plasmic membranes generally has a neutral net charge. Thus, our studies with anionic phospholipids (DMPG) reflect antimicrobial activity while studies with zwitterionic phospholipids (DMPC) illustrate hemolytic and/or cytotoxic activity. Although the hydrophobic HPA and anionic CM5 surfaces were not proper

Table 7: Antimicrobial and Hemolytic Activities of Plasticins

bacteria strain[a]	minimum inhibitory concentration (μM)					
	PBN2 KF	ANC KF	PD36 KF	PD36 K	PD36	ANC F
Gram-positive eubacteria						
S. aureus ATCC 25923	6.25	12.5	6.25	50.5	R	R
B. megaterium ATCC 9885	3.15	12.5	50.25	12.5	R	R
Gram-negative eubacteria						
E. coli 363 ATCC 11775	6.25	25	6.25	12.5	R	R
S. typhimurium CIP 6062	12.55	nd	25.25	R	R	R
E. cloacae ATCC 11775	12.55	R	12.5	100.5	R	R
	hemolysis (%)					
	PBN2 KF	ANC KF	PD36 KF	PD36 K	PD36	ANC F
50 μM	30	22	25	35	42	43
100 μM	70	48	50	71	75	65

[a] Bacteria strains were considered resistant (R) when their growth was not inhibited by peptide concentrations up to 100 μM.

Table 8: Peptide-Induced Inner Membrane Permeabilization of *E. coli* 363 ATCC 11775 Assessed with the DiS-C3(5) Probe[a]

	peptide concn (μM)	PBN2 KF (B)[b]	ANC KF (b)[c]	PD36 KF (b)[c]	PD36
MIC (μM)		6.25	25	6.25	>100
fluorescence (%)	5.0	0	0	40	nd
	12.5	51	0	100	nd
	75.0	49	0	95	0

[a] Membrane depolarization was monitored by an increase of diS-C3(5) fluorescence after the addition of peptide. Fluorescence (%) = $[(F_P - F_0) \times 100]/(F_T - F_0)$. [b] (B) = bactericidal effect. [c] (b) = bacteriostatic effect.
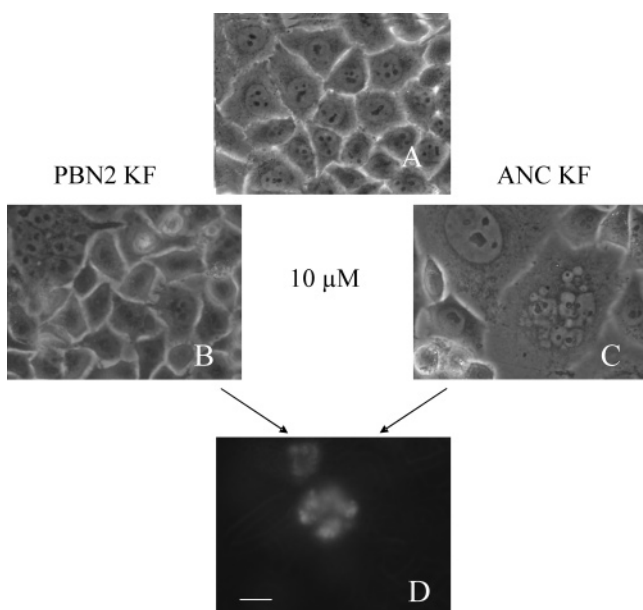

FIGURE 6: Imaging of Hela cells incubated for 24 h with peptides PBN2 KF (B) and ANC KF (C). (A) Control Hela cells. (D) Hoechst staining showing apoptotic bodies. The bar is 50 nm.

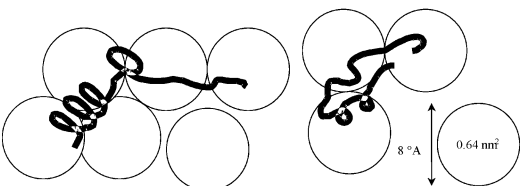membrane surfaces, they are suitable for the evaluation of the hydrophobic or hydrophilic counterpart.

Cationic plasticin structural analysis performed with DMPG vesicles by CD and FTIR (Table 2) evidenced an α-helix/β-structure ratio over or equal to 1 related to fast NH/ND-exchange kinetics (Figure 2) and bactericidal activity (Table 7). The use of hydrophobic HPA and anionic CM5 surfaces was necessary for accurate interpretation of SPR cationic plasticin adsorption data on anionic (DMPG) mimetic membrane. They were found to be orientated through their external hydrophobic helix surface toward the hydrophobic support (HPA), increasing the electrostatic repulsion between the positive K$^+$ charges. Additional peptide monomolecular layers were not observed. However, ANC KF plasticin presenting the highest β-structure content formed a nascent peptide bilayer at a concentration of 10 μM in accordance with its characteristic structural plasticity, and its aggregative properties were illustrated by multiple NH/ND-exchange behaviors (Figure 2).

The relationship between adsorption density and MIC was emphasized; particularly, the adsorption density was found to be insignificant at concentrations below the MIC (2). Readily soluble antimicrobial cationic plasticins were strongly adsorbed, with stable peptide–lipid interactions causing significant perturbations of the bilayer alkyl chains as seen by FTIR spectroscopy (Table 6). Cationic plasticins interacted with DMPG by decreasing the associated water content of the phospholipid heads (CO), replacing water molecules by peptides themselves (Table 5). This strongly suggests that they may act via other ways than the single breakdown of cytoplasmic membrane permeability. The interaction of the peptide with alkyl chains of DMPG phospholipids resulted in noticeable disordering of the acyl chain region of the fluid bilayer, probably as a consequence of peptide insertion (*18, 30*). Moreover, the D residues at position 16 (PD36 Ks) or 5 (ANC KF) promoted or weakened the sequestration time of the peptide by the lipid (Table 4). The absence of a D residue from PBN2 KF could explain its intermediate status. Peptides encompassing phenylalanine residues formed more dense PL* complexes with the DMPG bilayer (1.2 ± 0.05 ng·mm^{-2}) than did PD36 K (1 ng·mm^{-2}) (Table 4). The presence of aromatic residues clearly prolonged the contact time between peptide and membrane, allowing further structural rearrangements (*31*). The abilities of plasticins to act on lipid membranes were also related to their potentialities to cross membranes targeting thus cytoplasm or nucleus. Consequently, PBN2 KF, leading to the highest PL* complex density in a DMPG bilayer (Table 4), is believed to have the strongest capacity to cross membranes.

Plasticins varied substantially in their abilities to depolarize the membrane and showed that the membrane potential alterations occurred over various concentrations. No absolute correlation between the ability to permeabilize the cytoplasmic membrane and the antibacterial activity was shown. For example, PBN2 KF plasticin had good activity against *E.*

Table 9: PBN2 KF and ANC KF Features and Diagram of Their Putative Interactions with a Zwitterionic Surface[a]

	Feature	PBN2 KF	ANC KF
Structural polymorphism	α-helix content	40%	30%
	β-structure content (H-bond)	26%	31%
	NH content at 5 min	40%	30%
Lipid disturbance	Interface (1727/1742 cm^{-1} ratio)	1.6	1.7
	Alkyl chain ν_{AS} (CH) content	70%	72%
Adsorption process (DMPC)	PL* complex	15%	30%
Biological activity	Hemolysis (50 μM)	30%	22%
	Hela cells imaging	Nucleus fragmentation apoptotic bodies	Nucleus fragmentation apoptotic bodies
Diagram	Zwitterionic surface (Phosphocholine headgroups)		

[a] PL* complex density (ng·mm^{-2}) was evaluated by SPR measurements after 10 min desorption (see Table 4).

coli but presented a reduced ability to disrupt membrane potential. Moreover, this plasticin was bactericidal. In contrast, PD36 KF, presenting the peculiar mixture α-helix/β-structure (50%/50%) and bacteriostatic effect, seemed to have the greatest ability to dissipate the membrane potential (Table 8). Furthermore, ANC KF (75 μM, three times the MIC) had no effect on membrane potential diffusion but was bacteriostatic. These different behaviors for closely related peptides were certainly due to lipopolysaccharides (LPS) that are the major molecular component of the outer membrane of Gram-negative bacteria and serve as a physical barrier providing the bacteria protection from its surroundings (*32, 33*). As previously suggested by Wu et al. (*28*), the plasticin mechanism of action may involve some events other than the breakdown of the cytoplasmic membrane permeability.

Cationic plasticins were hemolytic on rat erythrocytes whereas PBN2 KF and ANC KF were found to be cytotoxic on Hela cells. However, our attempts to describe the molecular basis of cytotoxicity might not totally reflect the complexity of the erythrocyte membrane. Mammalian and fungal cells may also differ from prokaryote cells in their membrane sterol contents (*34*). It is noticeable that peptide−cholesterol interactions in plasma membrane have been proposed to inhibit (*35*) or enhance the formation of peptide structures inducing lysis.

FTIR experiments with DMPC vesicles showed that PBN2 KF and ANC KF interacted mainly with the lipid headgroups, which appeared to contradict the erythrocyte cytotoxic results. Actually, we assumed, like Epand et al. (*36*), that the interactions of peptides with model zwitterionic liposomes do not necessarily predict their hemolytic behavior.

This could be due to differences in the lipid−peptide contact time (15 min for FTIR experiments and 1 h for hemolytic tests) and/or the specific lipid compositions of the different types of membrane as above mentioned. Table 9 illustrates relationships between the structural polymorphism, lipid disturbance, membrane adsorption, and cytotoxic activity of the two representative peptides, PBN2 KF and ANC KF. Analysis of the lipid CO ester bands of the zwitterionic membrane showed that the binding of both peptides resulted in membrane dehydration and the formation of peptide−membrane hydrogen bonds, while the antisymmetric methyl bands in the ν(CH) stretching mode bands varied slightly, suggesting weak lipid disordering. PBN2 KF, mainly in α-helix conformation, was adsorbed to the same extent as dermaseptin B2 (*13*), while ANC KF underwent intermolecular associations on a hydrophobic surface. The density of the PL* complex formed by phosphatidylcholine vesicles and ANC KF (Table 4) showed that the residence time of this peptide was greater than that of PBN2 KF. In addition, the L/P molecular ratio (SPR data) for a DMPC bilayer, together with the putative conformation distributions, was used to deduce the self-organization of the plasticins PBN2 KF and ANC KF on zwitterionic biomembranes, with ANC KF about two times more densely packed than PBN2 KF (Table 9). ANC KF was cytotoxic for eukaryotic target cells, unlike magainin and dermaseptins that are poorly adsorbed onto zwitterionic surfaces (*1, 37−39*). The 1680−1780 cm^{-1} difference spectra confirmed these data and suggested that the binding of peptides containing two K and one F to the zwitterionic membrane was accompanied by membrane dehydration and the formation of peptide−membrane hydrogen bonding (Figure 3). Alternatively, there

could be a direct interaction between the peptide ϵNH_2 groups and the lipid CO ester through H-bonds (Table 5).

During bacterial attack, many peptides can be retrieved in the frog skin secretions. The resulting cocktail contains simultaneously neutral, anionic, and cationic peptides. We have already shown that inactive neutral peptides enhanced the activity of cationic peptides. Thus, neutral peptides could act as primary membrane-disturbing peptides by adopting a transmembrane orientation in synergy with cationic peptides (2). Neutral plasticins presented hemolytic activities which can be related to their self-association properties as assessed by low NH/ND-exchange kinetics (Figure 2). The lack of charge on neutral plasticins did not prevent their adsorption by hydrophobic−hydrophobic interactions (Figure 4) but could avoid the further rearrangement of neutral peptides in the bilayer to form PL* complexes with lifetimes compatible with biological activity. The disparity between ANC and PD36 neutral peptides underlines the essential role of the D residue position in these two plasticins.

No antimicrobial activity was observed if the α-helix/β-structure ratio is below 1, despite high α-helix content (40%). Neutral plasticins interacted with DMPC without perturbing either the interface (CO) or inside of the bilayer (alkyl CH), whereas they caused little perturbations at the interface peptide−DMPG vesicles as well as in the bilayer alkyl chains (Tables 5 and 6). However, the great plasticity of the neutral PD 36 and ANC F facilitated the formation of β-hairpin structures, allowing thus hydrophobic regions to be in contact with the hydrophobic support. The actions of the neutral plasticins on alkyl chains were more ambiguous, causing small perturbation possibly because of the high peptide concentration (2 mM) used for FTIR studies.

This study gives further information about many ways used by peptides to perturb biomembranes, leading to a biological activity as previously reported (2). Plasticins adopt various structural fittings in the vicinity of membrane mimetic supports. Neutral plasticins with strong β-structures revealed in the presence of phospholipid vesicles were weakly adsorbed in the range of antibacterial activity concentrations (micromolar). Nevertheless, for millimolar concentrations, they caused perturbations at the interface peptide−DMPG vesicles and in the bilayer alkyl chains, suggesting insertion into bacterial membranes. Cationic plasticins displayed multiple conformational transitions, including destabilized helix states, β-structures, and disordered state. The most soluble cationic plasticins were strongly adsorbed on DMPG, with stable peptide−lipid interactions inducing noticeable perturbations of bilayer alkyl chains, pointing out possible insertion into bacterial membranes. Some cationic plasticins were less adsorbed and characterized by less stable peptide−lipid interactions, causing membrane dehydration, formation of peptide−membrane hydrogen bonds, and little disturbances of lipid alkyl chains. They were shown to be cytotoxic for Hela cells, causing apoptotic bodies. This latter very stimulating result remains to be studied more precisely and particularly comforted by a set of experiments to characterize more precisely the potent apoptotic events. Further studies determining the action of several antimicrobial peptides as antitumoral agents will contribute to the development of new weapons in cancer treatment.

SUPPORTING INFORMATION AVAILABLE

Spectral decomposition method with the construction of standard spectra. This material is available free of charge via the Internet at http://pubs.acs.org.

REFERENCES

1. Lequin, O., Bruston, F., Convert, O., Chassaing, G., and Nicolas, P. (2003) Helical structure of dermaseptin B2 in a membrane-mimetic environment, *Biochemistry 42*, 10311−10323.
2. Vanhoye, D., Bruston, F., El Amri, S., Ladram, A., Amiche, M., and Nicolas, P. (2004) Membrane association, electrostatic sequestration, and cytotoxicity of Gly-Leu-rich peptide orthologs with differing functions, *Biochemistry 43*, 8391−8409.
3. van Kan, E. J., van der Bent, A., Demel, R. A., and de Kruijff, B. (2001) Membrane activity of the peptide antibiotic clavanin and the importance of its glycine residues, *Biochemistry 40*, 6398−6405.
4. Lorenzini, D. M., da Silva, P. I., Jr., Fogaca, A. C., Bulet, P., and Daffre, S. (2003) Acanthoscurrin: a novel glycine-rich antimicrobial peptide constitutively expressed in the hemocytes of the spider Acanthoscurria gomesiana, *Dev. Comp. Immunol. 27*, 781−791.
5. Sachetto-Martins, G., Franco, L. O., and de Oliveira, D. E. (2000) Plant glycine-rich proteins: a family or just proteins with a common motif?, *Biochim. Biophys. Acta 1492*, 1−14.
6. Wechselberger, C. (1998) Cloning of cDNAs encoding new peptides of the dermaseptin-family, *Biochim. Biophys. Acta 1388*, 279−283.
7. Duda, T. F., Jr., Vanhoye, D., and Nicolas, P. (2002) Roles of diversifying selection and coordinated evolution in the evolution of amphibian antimicrobial peptides, *Mol. Biol. Evol. 19*, 858−864.
8. Hagler, A. T., Stren, P. S., Sharon, R., Becker, J. M., and Naider, F. (1979) Computer simulation of the conformational properties of oligopeptides. Comparison of the theoretical methods and analysis of experimental results, *J. Am. Chem. Soc. 101*, 6842−6852.
9. Sreerama, N., and Woody, R. W. (2000) Estimation of protein secondary structure from circular dichroism spectra: comparison of CONTIN, SELCON, and CDSSTR methods with an expanded reference set, *Anal. Biochem. 287*, 252−260.
10. Surewicz, W. K., Mantsch, H. H., and Chapman, D. (1993) Determination of protein secondary structure by Fourier transform infrared spectroscopy: a critical assessment, *Biochemistry 32*, 389−394.
11. Goormaghtigh, E., Cabiaux, V., and Ruysschaert, J. M. (1994) Determination of soluble and membrane protein structure by Fourier transform infrared spectroscopy. III. Secondary structures, *Subcell. Biochem. 23*, 405−450.
12. Tatulian, S. A., Jones, L. R., Reddy, L. G., Stokes, D. L., and Tamm, L. K. (1995) Secondary structure and orientation of phospholamban reconstituted in supported bilayers from polarized attenuated total reflection FTIR spectroscopy, *Biochemistry 34*, 4448−4456.
13. Noinville, S., Bruston, F., El Amri, C., Baron, D., and Nicolas, P. (2003) Conformation, orientation, and adsorption kinetics of

dermaseptin B2 onto synthetic supports at aqueous/solid interface, *Biophys. J. 85*, 1196−1206.

14. de Loze, C., Baron, M., and Fillaux, F. (1978) Interactions of the CONH group in solution. Interpretation of the infrared and Raman spectra in relationship to secondary structures of peptides and proteins, *J. Chim. Phys. 75*.

15. Wantyghem, J., Baron, M. H., Picquart, M., and Lavialle, F. (1990) Conformational changes of Robinia pseudoacacia lectin related to modifications of the environment: FTIR investigation, *Biochemistry 29*, 6600−6609.

16. Blume, A., Hubner, W., and Messner, G. (1988) Fourier transform infrared spectroscopy of $^{13}C{=}O$-labeled phospholipids hydrogen bonding to carbonyl groups, *Biochemistry 27*, 8239−8249.

17. Cameron, D. G., Casal, H. L., and Mantsch, H. H. (1980) Characterization of the pretransition in 1,2-dipalmitoyl-*sn*-glycero-3-phosphocholine by Fourier transform infrared spectroscopy, *Biochemistry 19*, 3665−3672.

18. Lotta, T. I., Salonen, I. S., Virtanen, J. A., Eklund, K. K., and Kinnunen, P. K. (1988) Fourier transform infrared study of fully hydrated dimyristoylphosphatidylglycerol. Effects of Na^+ on the sn-1′ and sn-3′ headgroup stereoisomers, *Biochemistry 27*, 8158−8169.

19. Castano, S., Desbat, B., Laguerre, M., and Dufourcq, J. (1999) Structure, orientation and affinity for interfaces and lipids of ideally amphipathic lytic LiKj(i=2j) peptides, *Biochim. Biophys. Acta 1416*, 176−194.

20. Cooper, M. A., Try, A. C., Carroll, J., Ellar, D. J., and Williams, D. H. (1998) Surface plasmon resonance analysis at a supported lipid monolayer, *Biochim. Biophys. Acta 1373*, 101−111.

21. Myszka, D. G. (1997) Kinetic analysis of macromolecular interactions using surface plasmon resonance biosensors, *Curr. Opin. Biotechnol. 8*, 50−57.

22. Erb, E. M., Chen, X., Allen, S., Roberts, C. J., Tendler, S. J., Davies, M. C., and Forsen, S. (2000) Characterization of the surfaces generated by liposome binding to the modified dextran matrix of a surface plasmon resonance sensor chip, *Anal. Biochem. 280*, 29−35.

23. Casteels, P., Ampe, C., Jacobs, F., and Tempst, P. (1993) Functional and chemical characterization of Hymenoptaecin, an antibacterial polypeptide that is infection-inducible in the honeybee (*Apis mellifera*), *J. Biol. Chem. 268*, 7044−7054.

24. Sims, P. J., Waggoner, A. S., Wang, C. H., and Hoffman, J. F. (1974) Studies on the mechanism by which cyanine dyes measure membrane potential in red blood cells and phosphatidylcholine vesicles, *Biochemistry 13*, 3315−3330.

25. Wu, M., and Hancock, R. E. (1999) Interaction of the cyclic antimicrobial cationic peptide bactenecin with the outer and cytoplasmic membrane, *J. Biol. Chem. 274*, 29−35.

26. Kumar, A., Jose, G., Thomas, V., Unnikrishnan, N. V., and Nampoori, V. P. (2003) NIR to UV absorption spectra and the optical constants of phthalocyanines in glassy medium, *Spectrochim. Acta, Part A 59*, 1−11.

27. Cnubben, N. H., Blaauboer, B., Juyn, S., Vervoort, J., and Rietjens, I. M. (1994) A spectrophotometric assay for the detection of 2-aminophenols in biological samples, *Anal. Biochem. 220*, 165−171.

28. Wu, M., Maier, E., Benz, R., and Hancock, R. E. (1999) Mechanism of interaction of different classes of cationic antimicrobial peptides with planar bilayers and with the cytoplasmic membrane of *Escherichia coli*, *Biochemistry 38*, 7235−7242.

29. Yount, N. Y., Bayer, A. S., Xiong, Y. Q., and Yeaman, M. R. (2006) Advances in antimicrobial peptide immunobiology, *Biopolymers* (in press).

30. Aranda, F. J., Teruel, J. A., and Ortiz, A. (2003) Interaction of a synthetic peptide corresponding to the N-terminus of canine distemper virus fusion protein with phospholipid vesicles: a biophysical study, *Biochim. Biophys. Acta 1618*, 51−58.

31. Stahelin, R. V., and Cho, W. (2001) Differential roles of ionic, aliphatic, and aromatic residues in membrane-protein interactions: a surface plasmon resonance study on phospholipases A2, *Biochemistry 40*, 4672−4678.

32. Nikaido, H. (1994) Prevention of drug access to bacterial targets: permeability barriers and active efflux, *Science 264*, 382−388.

33. Papo, N., and Shai, Y. (2005) A molecular mechanism for lipopolysaccharide protection of Gram-negative bacteria from antimicrobial peptides, *J. Biol. Chem. 280*, 10378−10387.

34. Tytler, E. M., Anantharamaiah, G. M., Walker, D. E., Mishra, V. K., Palgunachari, M. N., and Segrest, J. P. (1995) Molecular basis for prokaryotic specificity of magainin-induced lysis, *Biochemistry 34*, 4393−4401.

35. Cruz-Chamorro, L., Puertollano, M. A., Puertollano, E., de Cienfuegos, G. A., and de Pablo, M. A. (2006) In vitro biological activities of magainin alone or in combination with nisin, *Peptides 27*, 1201−1209.

36. Epand, R. F., Lehrer, R. I., Waring, A., Wang, W., Maget-Dana, R., Lelievre, D., and Epand, R. M. (2003) Direct comparison of membrane interactions of model peptides composed of only Leu and Lys residues, *Biopolymers 71*, 2−16.

37. Kustanovich, I., Shalev, D. E., Mikhlin, M., Gaidukov, L., and Mor, A. (2002) Structural requirements for potent versus selective cytotoxicity for antimicrobial dermaseptin S4 derivatives, *J. Biol. Chem. 277*, 16941−16951.

38. Vogt, T. C., and Bechinger, B. (1999) The interactions of histidine-containing amphipathic helical peptide antibiotics with lipid bilayers. The effects of charges and pH, *J. Biol. Chem. 274*, 29115−29121.

39. Hicks, R. P., Mones, E., Kim, H., Koser, B. W., Nichols, D. A., and Bhattacharjee, A. K. (2003) Comparison of the conformation and electrostatic surface properties of magainin peptides bound to sodium dodecyl sulfate and dodecylphosphocholine micelles, *Biopolymers 68*, 459−470.

BI060999O